Proton versus cation selective transport of saccharide rim-appended pillar[5]arene PA-S artificial water channels

Iuliana Andrei, Wenzhang Chen, Marc Baaden, Stéphane Vincent, Mihail Barboiu

Proton *versus* cation selective transport of saccharide rim-appended pillar[5]arene PA-S artificial water channels

Iuliana M. Andrei,[†#] Wengzhang Chen,[‡¡#] Marc Baaden,[¤] Stéphane P. Vincent,[‡*] and Mihail Barboiu[†*]

[†] Institut Europeen des Membranes (IEM), Adaptive Supramolecular Nanosystems Group (NSA), University of Montpellier, ENSCM-CNRS, UMR 5635, 34095 Montpellier, France.
[‡] Department of Chemistry, Bio-Organic Chemistry Laboratory, University of Namur, Rue de Bruxelles 61, 5000 Namur, Belgium.
[¡] Actual address: Guizhou Medical University, 9 Beijing Road, Guiyang, 550004, China.
[¤] Université Paris Cité, CNRS, Laboratoire de Biochimie Théorique, 13 rue Pierre et Marie Curie, 75005, Paris, (France)

ABSTRACT: Transport of water across cell membranes is a fundamental process for important biological functions. Herein, we focused our research on a new type of symmetrical saccharide rim-functionalized pillar[5]arene PA-S artificial water channels with variable pore structures. To point out the versatility of PA-S channels, we systematically varied the nature of anchoring/gate keepers D-Mannoside, D-Mannuronic acid or Sialic acid H-bonding groups on lateral PA arms, known as good membrane adhesives, to best describe the influence of the chemical structure on their transport activity. The control of hydrophobic membrane binding – hydrophilic water binding balance is an important feature influencing the channels' structuration and efficiency for a proper insertion into bilayer membranes. The glycosylated -PA channels transport performances were assessed in lipid bilayer membranes, and they were able to transport water at high rates (~10^6-10^7 waters/s/channel within one order of magnitude as for aquaporins.) serving as selective proton railways with total Na^+ and K^+ rejection. Molecular simulation substantiates the idea that the PAs can generate supramolecular pores, featuring hydrophilic carbohydrate gate-keepers that serve as water-sponge relays at the channel entrance, effectively absorbing and redirecting water within the channel. The present channels may be regarded as a rare biomimetic example of artificial channels presenting proton *vs*. cations transport selectivity performances.

INTRODUCTION

One of the most important functions of biological membranes is its complex selective self-regulation of metabolites transport for the cell.[1] The transport is modulated by natural protein channels which work as selective filters.[2,3] Proton transfer is one of the most common biochemical processes holding a significant roles in the living cells.[4] the results is related to the acidification of interior of the cells, important in controlling physiological functions. A number of important diseases, resulting from dysregulation of protein channels, known as "channelopathies" can be treated with synthetic ion-channels that can have a great potential in anticancer treatments. Dedicated artificial proton channels are less common in recent literature. Even though many details of the proton transfer mechanism are still unresolved, the progress made showed that protons are travelling along membrane-bound waters assisted by protein functional groups, *via* a Grotthuss-type mechanism.[5–7] Actually, the diffusion of the proton mass is not required, as the migration of the proton charge along a wire of H-bonded water wires is sufficient.[8]

Inspired by biological channels, Artificial Water Channels-AWCs have been proposed with the hope to replicate the function of natural proteins, the Aquaporins involved in the selective water transport through bilayer membranes.[9] Molecular or self-assembled AWCs are constructed *via* covalent or reversible non-covalent bonds.[10] An optimal H-bonding of water within the channel is needed for selectivity, while less friction/interaction with the channel structuration is desired to increase the water permeability. The key to design AWCs is to construct functional pores with a specific aperture, that can sterically accommodate water clusters/wires in a selective manner. Having in mind such design strategies, the confined water can be used as protons' railways through the channels.

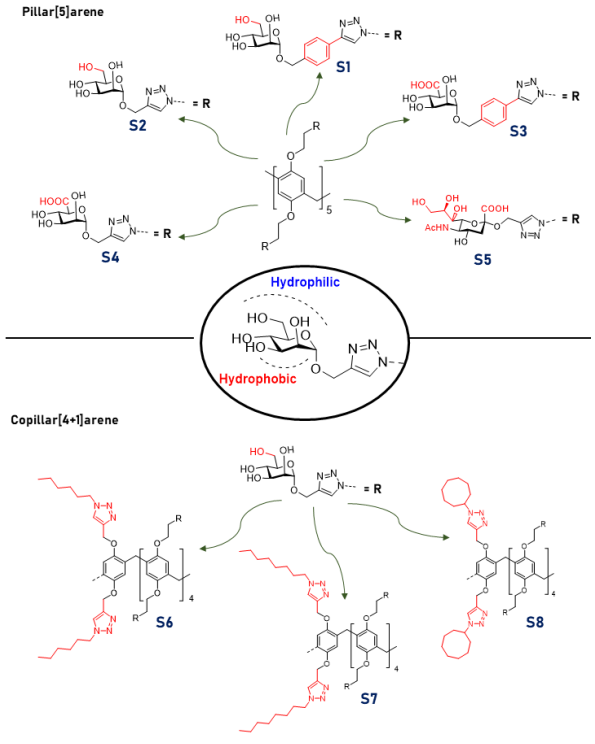

Figure 1. Chemical structures of saccharide homopillar[5]arenes (top) and copillar[4+1]arenes (bottom) and their structural variations (red). The D-mannoside configured carbohydrates display a hydrophobic membrane binding α-face and a hydrophilic water binding β-face.

During the last decade, a wide range of AWCs have been developed and studied with unique functional features for enhanced and synergetic water permeability and selectivity, such as I-quartets,[9–13] aquafoldamers,[14-18] dendritic dipeptides,[19,20] pillar[5]arenes[21-23] hydroxy channels[24,25] and more recently flourous nanorings.[26]

As a bioinspired approach, the aim is to learn from the biological protein scaffolds and implement the selectivity components in artificial molecules so that to control the channel build-up by constitutional self-organization. Aquaporins (AQPs) are protein channels involved in water transport through cell membranes. AQP is composed of an hourglass structure with a narrow constriction of 2.8 Å. Each water molecule transported forms H-bonds with the inner- protein and with adjacent waters. This way, opposite dipolar alignment of water molecules can control the water vs. proton transport selectivity of AQPs.[25,27]

It is of great importance to take into consideration four major factors regarding the construction of AWCs: a) the lipophilicity of the components, as this is ensuring their insertion into the lipid bilayer in order to form the channel; b) the overall length of the channel needs to optimally cross the phospholipid bilayer membrane thickness (~35-40 Å); c) the anchoring groups interacting with polar zwitterionic region of the lipids may control the orientation within membranes and d) the water/proton recognition sites pointing toward the inner channel may ensure the transport selectivity. The interactions between the recognition sites and water/protons should not be too weak, neither too strong. It must be an optimal association constant for obtaining good transport selectivity.[28,29]

Important investigations on constructing AWCs allowing a selective enhanced transport of water across the lipid membrane are related to the use of pillar[5]arene (PA) as a suitable macrocyclic platform for building channels. They were first synthesized by Ogoshi et al. in 2008.[29] Hou et al. reported in 2012 the first PA AWCs incorporated into lipid bilayers and encapsulating single water wires.[30] The PAs attracted the interest as they present multiple advantages like easy synthetic access, tunable size of cavity, easy fine-functional rims, self-assembly by H-bonding producing an expanded length-controlled tubular superstructure with amazing functions.[31-36] The significant progress obtained until now with the PA channels functionalized with peptide systems,[31-36] led to different attempts in functionalizing on both rims, which can show interesting results on water/proton translocation. Barboiu et al. have studied the crown-ether-pillar[5] arenes in selective transport of K^+ cations[14] and more recently described H-bonded dimeric rim-differentiated PAs[37] with great water transport activity and total ion rejection.[15] Vincent et al. already explored the complex multifunctional carbohydrate decorated PA-molecules,[38-42] that can also exhibit specific properties for applications in materials science[43] or chemical biology providing a great insights on the synthesis paths for designing such molecules and their strategic incorporation to optimize their drug delivery properties.[44]

Pursuing our endeavors in designing original supramolecular channels with efficient and selective transport properties, we recently got interested in the possibility of grafting saccharide residues on both rims of the PA platforms. From our previous experience we know that pillar[5]arene AWCs present a central hydrophobic cavity of ≈ 5 Å which is big enough to allow the passage of ions according to their hydration energy.[22] Molecular simulation show that partial permeation events can be detected through water empty hydrophobic pillar[5]arene PAP5 channels.[45] We anticipated that rim-functionalized saccharide- PA-S can form supramolecular pores with hydrophilic carbohydrate gate-keepers acting as water-sponge relays at the entry of the channels absorbing and redirecting water within the channel acting as proton railways. The saccharide components may also play an important role in channel adhesion to polar lipid heads leading to favorable orientation within the membrane. The objective of the present study is to make use of the membrane anchoring and water sponge gate-keepers behaviors of saccharide rim-functionalized pillar[5]arenes PA-S, towards the generation of active channels within lipid bilayer membranes. We anticipate that smaller pores with hydrophilic gate-keepers/anchoring saccharide arms grafted on pillar[5]arene core platforms are an interesting alternative to selectively accommodate highly permeating water channels.

RESULTS AND DISCUSSION

Design strategy. Herein, we concentrate our efforts on synthesizing saccharide rim-functionalized pillar[5]arene PA-S channels and on investigating their water/ion/proton transport performances through bilayer membranes. Homo-pillar[5]arenes and rim-differentiated pillar[5]arenes have been designed to construct AWCs and have shown high water transport activities. We noted that no copillar[4+1]arenes have been exploited to construct AWCs till now. We concentrated our efforts on synthesizing eight carbohydrate PAs *via* click chemistry (Figure 1).

In order to be able to point out the versatility of saccharide groups at the entry of the PA-platforms, as well as doing a systematic analysis of their transport activity and selectivity we considered different structural variations. As the size restriction plays a crucial role in the selectivity of water transport, the bulky hydrophilic head groups may both contribute to form size restriction and to form H-bonds with the phospholipid polar heads of the membrane. Carbohydrate might meet this tentative idea. Therefore, D-mannoside, D-mannuronic acid bearing carboxylic acid at 6-position, and sialic acid bearing a polyol group at 6-position and an amide group at 5-position which could play a role for both water binding/transport and interaction with the membranes were selected as the functional groups to decorate both rims. D-mannoside configured carbohydrates were selected for **S1**-**S4** and **S6**-**S8** because this sugar displays a hydrophobic α-face and a hydrophilic β-face (Figure 1). Therefore the α-face can interact with the lipid bilayer in a non-repulsive manner while the β-face displays multiple H-bonding possibilities with the transported water molecules. Sialic acid appended **S5** was also selected because its carboxylic acid is located close to the anomeric position, thereby deeper inside the channels, which may significantly impact the transport properties.

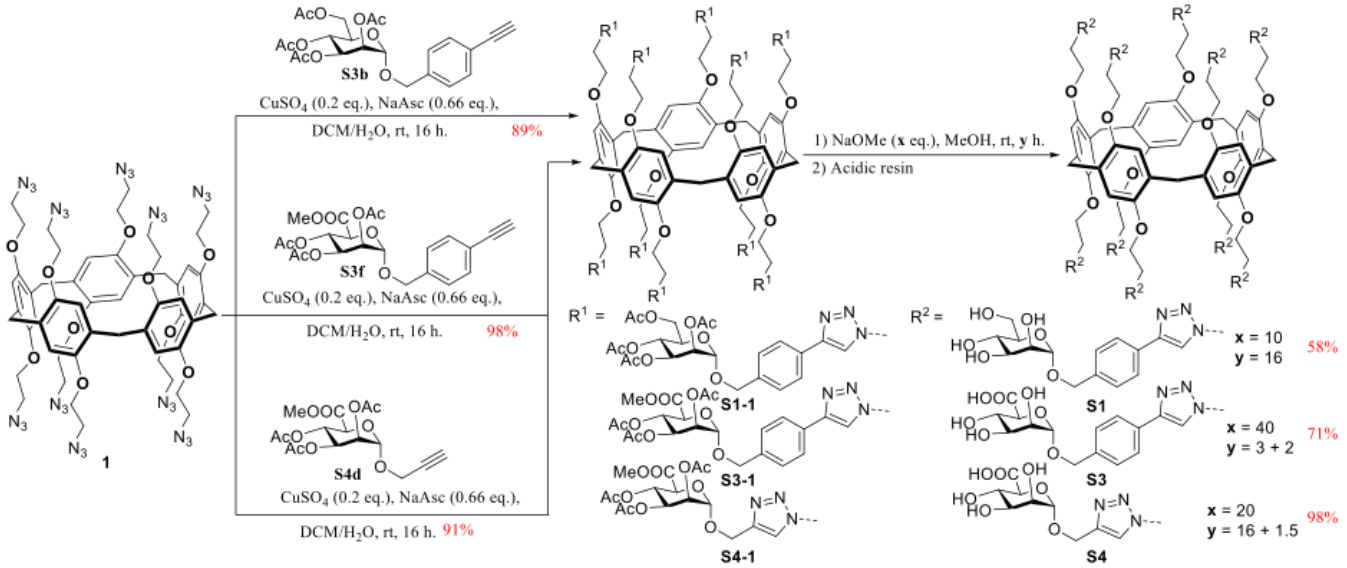

Scheme 1. Synthetic routes of **S1**, **S2** and **S4** artificial water channels.

The choice of carbohydrate end groups in **S1**-**S5** is primordial as we use variable moieties such as gate keepers' groups that are able to selectively interact as a sponge with water or protons in a very specific way and to ensure the increase of water/proton permeability. The phenyl ring can be easily introduced by simple glycosylation with the corresponding glycosides. It should allow us to compare two structural features: the presence/absence of the hydrophobic phenyl ring. The triazole ring connection between carbohydrate end groups and PA platforms on both rims may be of utmost importance as water/proton relays within the channels able to achieve the natural selectivity of protein channels.[46] Out of all these compounds, three PAs are copillar[4+1]arenes **S6**-**S8** obtained by regioselective bis-functionalization of pillar[5]arenes.[47]

Indeed, copillar[4+1]arenes could allow the introduction of different functions onto the central scaffold with two hydrophobic hexyl, octyl and cyclo-octyl tails conferring increased hydrophobicity to such eight glycosylated PAs at the interface with the lipid bilayer membrane. They will allow us to compare the effect of the length of the alkyl (C6/C8) and the presence of cycloalkyl (C8/cyclo C8) arms on the increased membrane solubility of these new copillar[4+1]arenes.

It is of great importance to note that thickness of the bilayer membrane (~35-40 Å) is quite similar to the length of one PAs molecules **S1**-**S8** that assemble into functional water-permeable channels in liposomes and increase the overall water permeability with respect to the background lipid permeability.

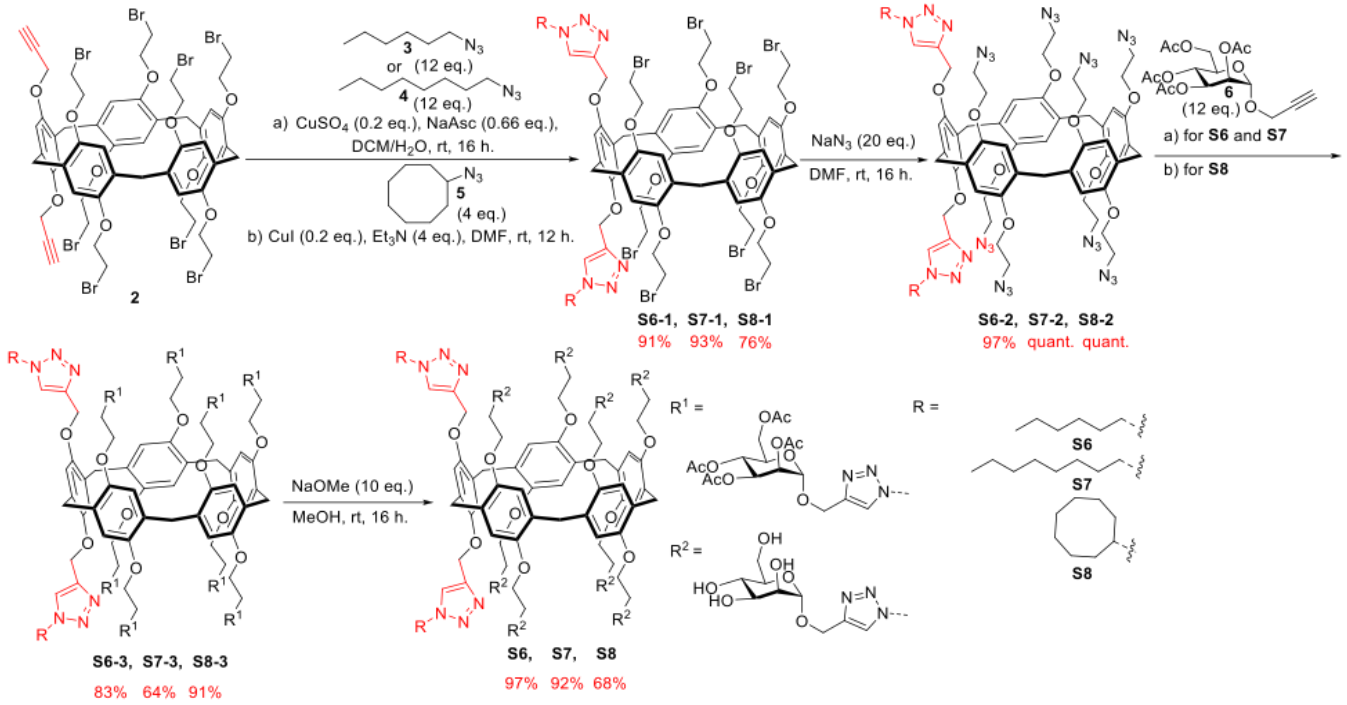

Scheme 2. Synthetic routes of S6, S7 and S8 artificial water channels.

To verify our hypotheses, the chemical syntheses of PAs molecules **S1-S8** were then carried out. The known homo-pillar[5]arene **1**[46] and copillar[5]arene **2**[47] were chosen as the core scaffolds for fabricating the saccharide rim-appended homo- (Scheme 1) and co-pillar[5]arene (Scheme 2), respectively. For the first class, homo-pillar[5]arenes **S1**[42] and **S2** were synthesized according to a known synthetic pathway.[48] An excess amount of clickable mannoside **S3b** (Scheme S1), mannuronic acid derivatives **S3f** (Scheme S1) and **S4d** (Scheme S2) were coupled to decaazidated pillar[5]arene **1** with a catalytic amount of $CuSO_4$ in a mixed solvent system (DCM/H_2O, 1:1). After stirring at room temperature overnight, the corresponding precursors **S1-1**, **S3-1** and **S4-1** were generated in 89%, 98% and 91% yields, respectively, after a simple silica gel chromatography purification. A Zemplén deprotection allowed to remove all acetyl groups and **S1** was successfully obtained with a moderate yield of 58% after treatment with an acidic resin.

For the mannuronates **S3** and **S4,** water was added to hydrolyze the methyl esters of **S3-1** and **S4-1** before the neutralization step with the acidic resin, to generate the fully deprotected homo-pillar[5]arenes **S3** and **S4** in 71% and 98% yield, respectively. Due to the presence of the phenyl rings, the fully deprotected molecules **S1** and **S3** display poor solubility properties which may lower the yields of the final steps. For the second series of copillar[4+1]arenes, the desired saccharide rim-appended co-pillar[5]arenes **S6**, **S7** and **S8** were prepared by a sequence including two CuAAC, an intermediate azidation and a final Zemplén deprotection. Briefly, twelve equivalents of the clickable hydrophobic tails **3**[49] and **4**[50] were coupled to copillar[5]arene **2** under classical click conditions (copper sulfate (0.2 eq.) and sodium L-ascorbate (0.66 eq.)) to give **S6-1** and **S7-1** in 91% and 93% yields, respectively.

Then, the two brominated intermediates were azidated, which allowed the grafting of mannoside **6** by another click reaction.[34] Accordingly, the subsequent full de-acetylation gave the desired artificial water channels **S6** and **S7** with an overall yield of 71% and 55%. Final artificial water channel **S8** was thus obtained in 47% yield from copillar[5]arene **2** in 4 steps. The preparation of biscyclooctyl artificial water channel **S8** from azidocyclooctane **5**[51] required a slightly modified procedure. In that case, CuI was used as a catalyst for the two click reactions. Final artificial water channel **S8** was thus obtained in 47% yield from copillar[5]arene **2** in 4 steps.

Sample Preparation for Liposome Transport Experiments. The PA **S1-S8** channels were reconstituted into egg yolk phosphatidylcholine (EYPC) lipid vesicles (100 nm in diameter) at different molar ratios of compound to lipids (mCLR = 1.54%, 4.62%, 9.24%, 12.33%, 15.41%), except for **S1** (mCLR = 0.15%, 0.39%, 0.77%, 1.16%, 1.54%) which presented low solubility in PBS (10 mM, pH = 6.4) and started precipitating above 1 mM. The compounds **S1-S8** were simply solubilized into dimethyl sulfoxide solution (DMSO) and added to the preformed vesicle suspension (see Supportive Information for details).

Water-Transport Experiments. The water transport through lipid bilayer membrane was performed using the stopped-flow technique, based on mixing two solutions of different concentrations. This method allows the testing of **S1-S8** on the same vesicle substrate. The preformed vesicle solution containing PA-S channels is exposed to outwardly directed osmotic pressure gradients, which conducts to the liposomes' shrinkage (Figure 2a).

Table 1. The highest net and single-channel permeability values corresponding to their mCLR for each carbohydrate PA-channel.

PA-channel	mCLR, %	Net permeability, μm/s	PS, molecules H_2O/s/channel
S1	1.16	0.79	$8.16 \cdot 10^6$
S2	15.41	8.75	$8.93 \cdot 10^6$
S3	15.41	9.15	$9.33 \cdot 10^6$
S4	9.24	4.39	$6.70 \cdot 10^6$
S5	15.41	4.66	$4.75 \cdot 10^6$
S6	15.41	6.55	$6.68 \cdot 10^6$
S7	15.41	8.43	$8.60 \cdot 10^6$
S8	12.33	11.78	$1.43 \cdot 10^7$

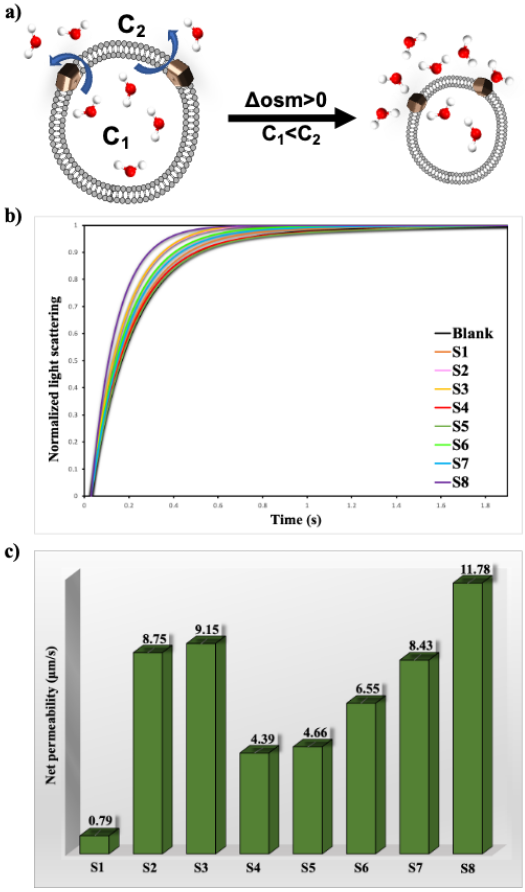

Figure 2. a) Schematic representation of liposomes' shrinkage under hypertonic conditions, in which the outside concentration is bigger than the inside concentration forcing the water molecules to pass through PA-channels to equilibrate the system; b) The stopped-flow light scattering traces of liposomes containing different PA-channels at mCLR = 1.16% (**S1**), 15.41% (**S2**), 15.41% (**S3**), 9.24% (**S4**), 15.41% (**S5**), 15.41% (**S6**), 15.41% (**S7**), 12.33% (**S8**); c) Highest net permeability values obtained from the light scattering traces of liposomes at mCLR = 1.16% (**S1**), 15.41% (**S2**), 15.41% (**S3**), 9.24% (**S4**), 15.41% (**S5**), 15.41% (**S6**), 15.41% (**S7**), 12.33% (**S8**).

Under hypertonic conditions driven by outwardly 10 mM PBS (pH = 6.4) comprising 100 mM KCl competitive osmolyte, the shrinkage of liposomes increases the light-scattering signal (Figure 2b). It was observed that the net permeabilities increase when mCLR ratios increase until it reaches a saturation point (Table S1).

S1 containing the 1-*O*-phenyl-D-mannosyl residues present the lowest water net permeability at 0.75 μm/s, most probably related to its observed low solubility in membrane, considering that all the other systems tested had their net permeability values in the range of 2.2 – 6.3 μm/s at the same mCLR = 1.54% (Table S1). Then when D-mannunronic, sialic acid and D-mannose residues were used without phenyl connectors in **S4**, **S5** and **S6** respectively they become more permeable compounds presenting a net permeability between 4.30 μm/s to 6.50 μm/s for the same mCLRs (Table S1).

The mannosylated compounds **S2**, **S7** presenting similar permeabilities of 8.75 μm/s, 8.43 μm/s together with the 1-*O*-phenyl-D-mannuronic acid in **S3** getting 9.15 μm/s respectively seem to have an optimal hydrophobic membrane / hydrophilic channel balance to get inserted at high mCLR = 15.41% (Figure 2c) and transporting water with higher permeabilities.

The highest net permeability of 11.8 μm/s is shown to be at mCLR = 12.33% for **S8** (Figure 2c), which implies that the copillar[4+1]arene with mannose and cyclooctyl residues presented the best combination in terms of membrane insertion capacity and water transport activity.

We noted that D-mannose arms presenting a hydrophilic/hydrophobic structure are better candidates for both water binding and transport along with better insertion/solubility in the membrane. In regard to the copillar[4+1]arenes (**S6**, **S7**, **S8**) grafted with the same D-mannose arms alternating just the length of the alkyl chain (**S6**, **S7**) / cycloalkane (**S8**) it can be observed that an optimal length for the octyl chain, while the net permeability values increase significantly, reaching the highest value of all tested compounds of ~11.8 μm/s for cyclo-octyl chain in **S8** (Table 1).

We further calculated the single-channel permeability (Ps) of each PA-channel[12] and it was observed that the values obtained are more or less the same of ~1.2 ± 0.2 x 10^7 water molecules/s/channel that are only one order of magnitude lower than that of aquaporin (~10^8 water molecules/s/channel)[27] (see Supportive Information for details). Increasing the mCLRs will induce slight decrease of single-channel permeability, without any changes of the level of magnitude (Table S1). This tendency of Ps for dropping values can be explained by progressive higher aggregation and lower solubility of the PA-channels when added in high concentrations. To prevent the aggregation, lower concentrations are preferred to incorporate the PA-channels into lipid bilayer membranes. It can be noticed that the net permeabilities reported before are the simple consequence of the overall solubility of the compounds in the bilayer membrane.

Cation and Proton-Transport Experiments. The ion (Na^+ and K^+) transport properties across bilayer membranes incorporating **S1-S8** channels are reconstituted into egg yolk phosphatidylcholine (EYPC) lipid vesicles with a diameter of 100 nm at the same mCLRs as used to assess the water transport (see Supportive Information for details). Ion transport activity was assessed using standard HPTS - (8-hydroxypiren-1,3,6-trisulfonic acid, trisodium salt) fluorescence assays, based on the balance between the acidic form and basic form of HPTS. The acidic form is predominant at pH = 6.4, while the basic form predominates at pH = 7.4 (Figure 3a). The two forms of the fluorescent substance have two different excitation wavelengths, namely at 405 nm for the acidic form and 450 nm for the basic form, and both forms have an emission wavelength at 510 nm. Tests using HPTS are ideal for characterizing artificial ion transport systems, as this is the least selective type of test and produces a signal for most transport mechanisms.[52-55]

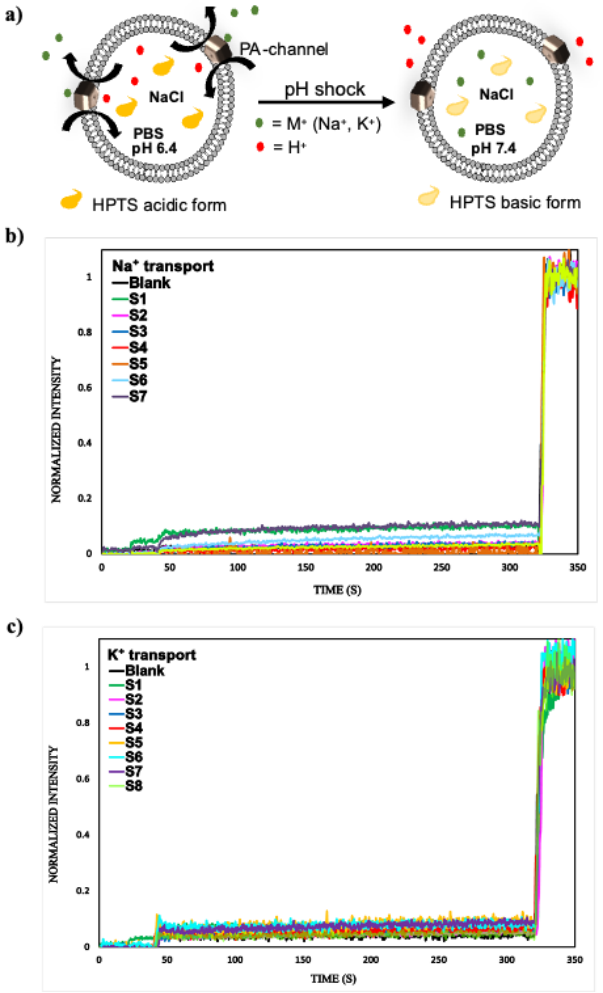

Figure 3. a) Schematic representation of antiport M^+/H^+ in liposomes; b) Comparison of Na^+ transport activity expressed as normalized fluorescence intensity of 1 mM **S1** and 10 mM **S2-S8** channels in the extravesicular media containing 100 mM NaCl in 10 mM PBS. c) Comparison of K^+ transport activity expressed as normalized fluorescence intensity of 1 mM **S1** and 10 mM **S2-S8** channels in the extravesicular media containing 100 mM KCl in 10 mM PBS.

When tested with NaCl or KCl on external buffer, the **S1-S8** did not present any activity after the compound injection at t = 20 s, the internal pH remains stable and even after the creation of a pH-gradient, applied at t = 40 s, there was not an increase of the internal pH, remaining quasi-stable, independent on the nature of the channel or transported cation (Figures S60-S61). These HPTS dose-response experiments show a constant absorbance behavior. The Na^+ and K^+ cations are not transported through the PA-channels and the pore structuration is

not effective to inducing Na^+ or K^+ / H^+ antiport conductance states along the assembled channel for any of the studied concentrations (Figure 3b, c).

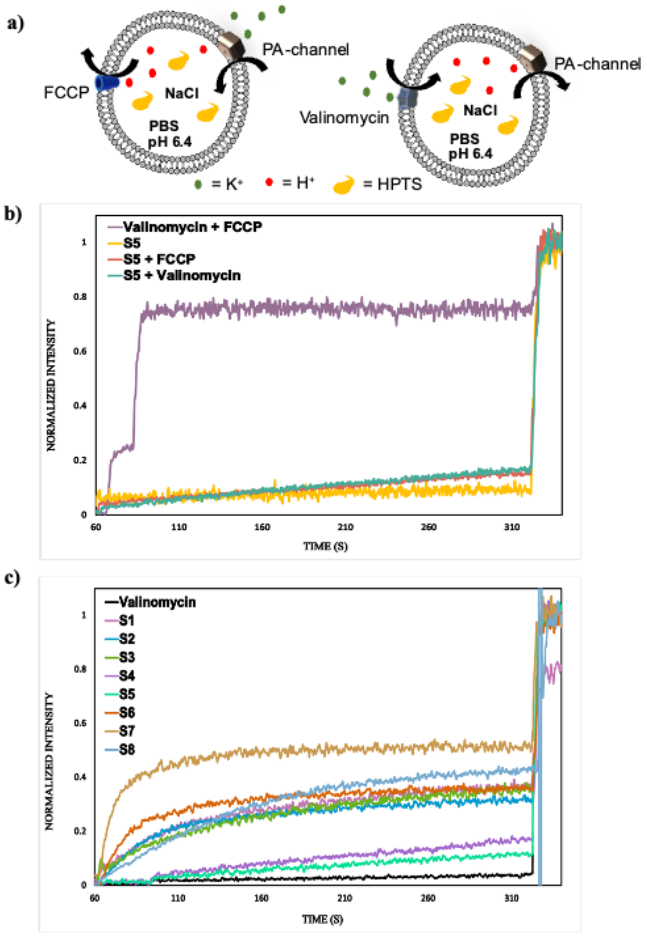

Figure 4. a) Schematic representation of proton transport activity in lipid bilayer membranes containing in the extravesicular medium 100 mM KCl. Liposomes incorporating HPTS (fluorescent dye) and NaCl (100 mM) in PBS solution (10 mM, pH 6.4) showing the membrane's polarization via FCCP as H+ carrier and valinomycin as K^+ carrier and their K^+/H^+ antiport mechanism. b) Ratiometric fluorescence curves (I/I0) of the transport experiments coupling **S5** channels at their highest concentration (10 mM) in the absence and presence of FCCP. c) Comparison of proton transport activity expressed as ratiometric fluorescence curves (I/I0) of 1 mM **S1** channels and 10 mM **S2-S8** channels coupled with valinomycin as K^+ carrier.

To complement these results, proton transport measurements were performed to check K^+/H^+ antiport (Figure 4a). We subjected the liposomes containing different concentrations of **S1-S8** channels in the presence of carbonyl cyanide 4-(trifluoromethoxy)-phenylhydrazone (FCCP) and monitored the fluorescence change over time (see Supporting Information for details). FCCP is widely known as a proton transport carrier so it would determine the PA-channels to transport K^+ cations across the channel in case they are K^+ selective. The electrogenic antiport experiments using FCCP – H^+ (50 0 nM) carrier and KCl on external buffer did not show any differences from the previous results (Figure S62). Potential K^+ transport *via* PA-channels is totally inactive, thus we can consider the channels' structuration is not allowing efficient transport for K^+ cations (Figure 4b). Further assays were performed using electrogenic membrane polarization using valinomycin as a K^+ carrier (Figure S63). The HPTS proton tests performed for **S1-S8** compounds using valinomycin – K^+ (500 nM) carrier generated K^+/H^+ antiport rates through the channels (Figure 4b).

It was observed that the fluorescence intensity was increasing with the increase of concentration of the compounds in the membrane, implying that high H^+ translocation across the bilayer membranes occurs when more compound was added. Valinomycin-K^+ cation transport across the membrane would accelerate the H^+ transport through the channels (Figures S62-S63).

All compounds show reasonable proton transport activities by coupling of valinomycin with the **S1-S8**, channels and generated a strong activity (I >0.4 for **S7**, **S8**) to medium-low (I = 0.2-0.4 for **S1**, **S2**, **S3**, **S6**) or very low (I < 0.2 for **S4**, **S5**) (Figure S63). Contrary to cation diffusion, proton translocation is a structural diffusion through water clusters and in OH-channels case is strongly correlated with the water transport performances and channel insertion in bilayer membranes, as protons can translocate principally via directional H-bonds of water clusters stabilized by the channels. The most performant PA-**S8** channels are again observed as the best proton channel within this series.

Molecular dynamics simulations of S3 and S8 channels in bilayer membranes. Exploratory molecular dynamics simulations were performed to investigate the properties of the most active compounds **S3**, a pillar[5]arene, and **S8**, a copillar[4+1]arene, when introduced into a fully hydrated lipid bilayer membrane. Particular attention was paid to the ability of the compounds to form water channels that allow cross-membrane water or proton transport. These compounds were part of a series and represented the best performing variants in terms of permeation. Here we examine how a single such molecule behaves in a membrane environment composed 100% of PC phospholipids. Such a supramolecular construct is difficult to model accurately using force field representations, and here we attempt to explore an initial plausible model. We use a simple, fully hydrated model "membrane" composed of pure POPC, mimicking the experimentally used EYPC liposome (Table S1, Figures S64, S65).

We observed a stable water wire for both compounds, exhibiting comparable features, as shown in **Figure 5**. The wire forms with a wide opening at both mouths but a single-file connected water chain in the center of the pillar-arene. The sugar-coated extremities of **S3** and **S8** are oriented with hydrophobic part toward membrane or interacting with water/phosphate groups or the lipids. They are sustaining a ramified water wire network/reservoir leading into and through the core of the pillar-arenes. **S3** provides a slightly longer central channel, extending on average ~6.6 Å further into the membrane headgroups than **S8**, and shielding the water wire from the hydrophobic membrane environment on a longer segment. As both compounds interact strongly with the bilayer, the result of the different membrane span is a marked thinning of the bilayer width close to the insertion site of the shorter **S8** compound, to accommodate for its dimension. This is shown in **Figure S66**.

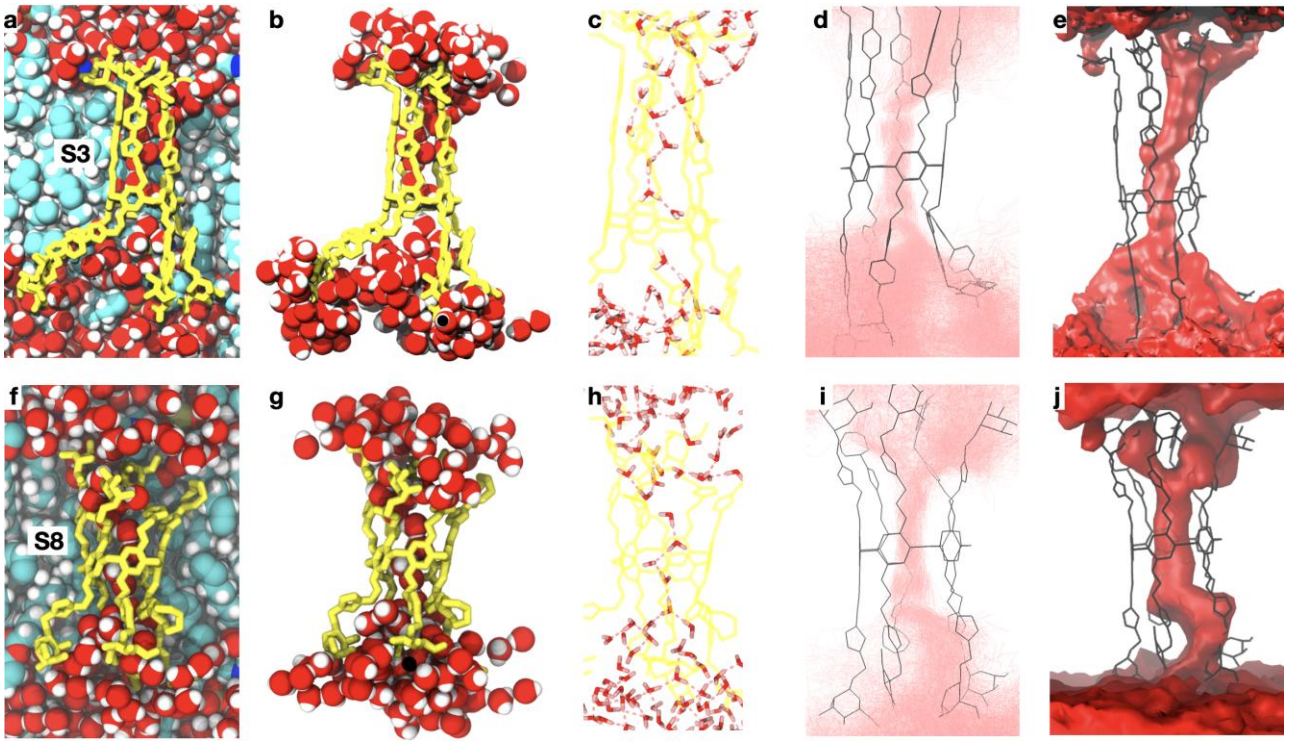

Figure 5. Detailed views of the penetrating water network in the final snapshots of simulations **S3** and **S8**. In **a** and **f**, the embedding of the pillar-arenes in their surroundings with the intruding water is shown in van der Waals representations for **S3** and **S8**, respectively. The pillar-arenes are shown in yellow. In **b** and **g**, everything except the pillar-arenes and the water within 5 Å of it is removed for clarity. To highlight the hydrogen bonding network, the pillar-arene framework is shown in **c** and **h** as thin transparent lines. The hydrogen bonds within a distance criterion of 3.5 Å and an angular range of 30 degrees are shown as pink dashed lines, with the hydrogen atoms colored pink as well, for better visibility. All hydrogen bonds for the full production run trajectories are shown as superoposed pink lines after alignment of the trajectory on the central arene ring in **d** and **i**. The oxygen density of the water averaged on the whole production trajectory is shown in **e** and **j** to make the branching at the mouths more apparent.

We then conducted a closer examination of the interactions between the membrane and the pillar-arenes. On average, the **S3** compound forms 15.6 hydrogen bonds with the surrounding lipid molecules, while **S8** forms 21.0 hydrogen bonds. Hydrogen bonding fluctuates more significantly for S8 as depicted in **Figure S71**. These hydrogen bonds are further illustrated in **Figure S72**. Noticeable lipid density accumulates around the compounds, with lipids enveloping them at specific sites. A handful of lipid molecules maintain a close association, seemingly stabilizing the pillar-arene conformation. This arrangement ensures sufficient spacing for water to enter through the expanded mouth regions. We proceeded to characterize the tunnel pore formed by the pillar-arenes. Utilizing an averaged structure across the entire production trajectory, we employed the MOLEonline service to calculate the tunnels depicted in Figure 6. The length measures 28.4 Å for **S3** and 35.9 Å for **S8**, which exceeds the actual extension of the compounds, taking into account its non-linear nature. The bottleneck diameter for **S3** is 2.6 Å, and for **S8**, it is 2.0 Å. While a few bottlenecks are present, the predominant portion of the tunnel boasts ample width to accommodate a water wire. Even the narrower bottlenecks have the potential to be bridged by hydrogen bonds. The pore profile furthermore provides a rationale for the observed ion rejection with respect to Na+ and K+ transport, as they would force a solvated ion to shed it's solvation shell, with no alternative favorable pore lining inside the pillar-arene. This feature does not prevent proton transport through a Grotthus mechanism. In a manner evocative of ion channels, these pillar-arene structures may inherently exhibit a probability of opening that isn't characterized by sustained, continuous permeation. Capturing such an inherent open probability in simulations proves challenging. Within this context, our ongoing investigation squarely focuses on open states, fully acknowledging that the precise determination of the equilibrium between open and closed states lies beyond the scope of this computational exploration. To ensure this approach's effectiveness, we meticulously and progressively equilibrated the water-filled channels, stabilizing them for the production phase. It is important to note that the experimental conditions entail an osmotic pressure conducive to transport—a factor absent in our simulations. In a modest attempt to emulate this osmotic pressure, our chosen strategy revolves around maintaining the channel in an open configuration. When considering ion rejection, a rigorous approach to investigate the selectivity mechanism between Na^+/K^+ and protons would involve calculating the potential of mean force associated with such a process. However, this calculation falls outside the current scope of our study. Nevertheless, relying on the analysis of pore geometry, it becomes highly likely that the selectivity mechanism is rooted in the barrier preventing ion dehydration. This barrier is made even more stringent by the absence of favorable groups within the arene interior, in contrast to ion channels such as those offering an alternative solvation environment within their selectivity filter.

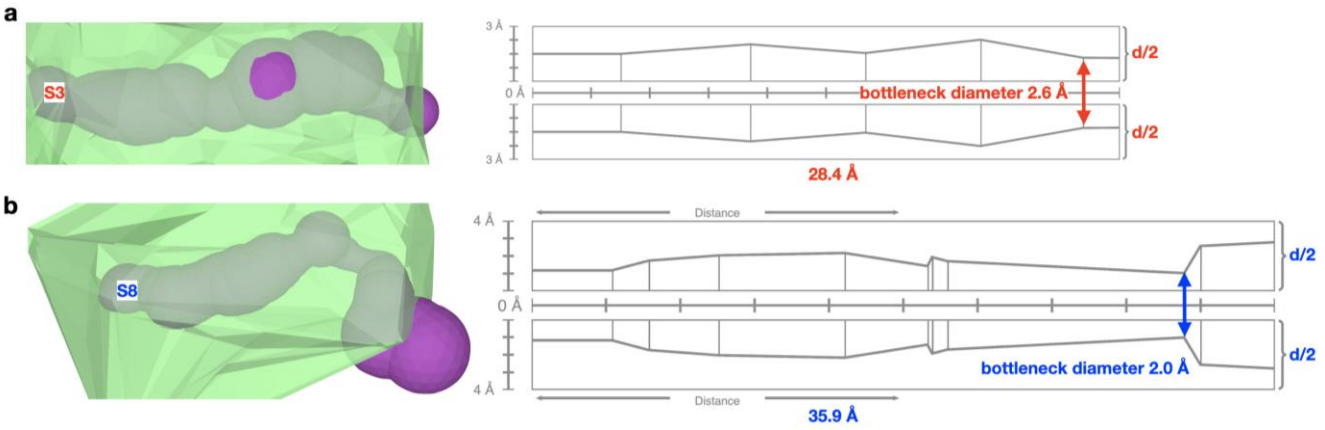

Figure 6. Analysis of the inner tunnel forming the water passageway is conducted for compounds **S3** (panel **a**) and **S8** (panel **b**). The tunnel is depicted in magenta, with a focus on assessing its diameter across its length, which is further quantified. The narrowest constriction diameter is highlighted. This analysis is performed on an averaged structure derived from each production run, utilizing the MOLEonline service.

CONCLUSIONS

Over the past years, artificial ion channels have been extensively studied, while the very young field of artificial water channels is still far from being fully explored. Peptide-appended pillar[5]arenes were previously described as efficient artificial water channels,[56,57] pillar[5]arene core representing a suitable scaffold for grafting functional groups to enhance their water selectivity. The approach considered in designing new artificial water systems is a biomimetic one, striving to replicate the function and not the structure of certain natural channels. Taking into consideration this premise, here we describe saccharide rim-functionalized pillar[5]arene artificial water channels **S1-S8** bearing D-mannose, D-mannuronic acid or sialic acid gate-keepers or anchoring membrane points at the entry of the PA-channels. The PA-S channels present water transport performances within one order of magnitude as the transport rates for aquaporins. This study demonstrates that the control of hydrophobic – hydrophilic balance is an important feature for a proper insertion into bilayer membranes. Slight structural modifications to the saccharide number and disposition of functional groups surrounding the hydrophilic cavity of the channels or the increase of the concentration of the compounds in the membrane, including hydrophobic tails on the PA backbone can drastically change the water permeability. The role of sugars as gate keepers was substantially proved by molecular simulations as they strongly contribute to the formation of water reservoirs at the entries of the channels, while the central pillararenes ring may be considered as a selectivity filter as in Aquaporins.[7]

The concluding assumption is that mannoside heads and hydrophobic cyclooctyl would lead to the most performant structures in a membrane environment, providing railways for water translocation and selective proton vs; cation transport through the transient water clusters.

The analysis of molecular dynamics simulations for both compounds has revealed the formation of selective water wires across the membrane, guided by the pillar-arene scaffold. These wires provide efficient pathways for a Grotthus mechanism that facilitates effective proton transport, coupled with complete Na+ rejection. The water wires are optimally connected through hydrogen bonds, thereby indicating a high potential for efficient proton transport and outstanding performance. The stability of these hydrogen-bonded water wires, observed in both the homopillar[5]arene **S3** and the copillar[4+1]arene **S8**, serves as a noteworthy example of artificial proton channels, a rarity in such compounds. The majority of hydrogen bonding within the channel is concentrated around the mouth regions, aiding in selective compound permeability. Conversely, interactions within the core of the channel exhibit minimal friction and interaction with the channel structure, confirming a relevant design principle aimed at enhancing water permeability. The saccharide components play a pivotal role in anchoring the channel to polar lipid headgroups, promoting favorable orientation and strong integration within the membrane. Both **S3** and **S8** compounds exhibit the highest permeabilities in the series that was experimentally tested, a finding consistent with our analysis of robust membrane insertion and the formation of stable water pathways with distinctive characteristics. Their geometry is finely tuned, with bottlenecks just narrow enough to control a single water wire. These compounds possess the advantageous combination of balanced hydrophobic membrane interactions and hydrophilic channel properties, ensuring a high rate of membrane insertion and enabling efficient water transport.

More importantly, salt rejection is almost total. Furthermore, proton vs cation selectivity of the PA-S channels is of tremendous importance correlating adaptive dynamic translocation of waters inside the channels correlating on water-conduction behaviors previously observed with PA-S channels within membranes.

Ion-induced proton co-transport in biological channels can efficiently acidify the interior cell environments to accelerate or control the physiological functions. Developing artificial ion channels helps in understanding the structure−function of natural protein and contributes to the development of potential treatments related to severe ion channelopathies.

Proton selectivity and low-pH gating are the key functions of Influenza A M2 proton channel,[58] or to the light-driven proton transport of proton pumping by microbial rhodopsins.[59]

Nevertheless, artificial proton channels are rarely described in literature.[9,11, 60,61] Although there is some variability compared

with the natural proteins, biomimetic I-quartet channels reported by our group a decade ago remained long time as unique proton selective transporters *via* artificial water channels,[9,11] while nowadays new discoveries in this field are being made. Realizing the exclusive proton flux through lipid bilayers remains a challenging task.[60,61]

Importantly, in this work we discovered by serendipity a simple design strategy for preparing highly selective artificial proton channels by precisely modulating the anchoring/gate keepers of the synthetic PAs scaffold.

ASSOCIATED CONTENT

Supporting Information

Materials and methods, NMR and ESI MS spectra analysis of studied compounds, TGA and DSC analysis, FTIR, DLS, XRD powder, SCXRD, XRD1 beamline of Elettra synchrotron, transmembrane transport experimental and molecular dynamic simulation, Molecular simulations details and supplementary figures for simulations. Supporting video animations can be founded at : http://www.baaden.ibpc.fr/v2/hidden/ja-2023-063353.html.

The Supporting Information is available free of charge on the ACS Publications website.

AUTHOR INFORMATION

Corresponding Authors

* **Mihail Barboiu** - Institut Europeen des Membranes (IEM), Adaptive Supramolecular Nanosystems Group (NSA), University of Montpellier, ENSCM-CNRS, UMR 5635, 34095 Montpellier, France. Email: *mihail-dumitru.barboiu@umontpellier.fr*

* **Stéphane P. Vincent** – Department of Chemistry, Bio-Organic Chemistry Laboratory, University of Namur, Rue de Bruxelles 61, 5000 Namur, Belgium. Email: stephane.vincent@unamur.be

Authors

Iuliana M. Andrei - Institut Europeen des Membranes (IEM), Adaptive Supramolecular Nanosystems Group (NSA), University of Montpellier, ENSCM-CNRS, UMR 5635, 34095 Montpellier, France.

Wengzhang Chen - Department of Chemistry, Bio-Organic Chemistry Laboratory, University of Namur, Rue de Bruxelles 61, 5000 Namur, Belgium. Actual address: Guizhou Medical University, 9 Beijing Road, Guiyang, 550004, China.

Marc Baaden - Université Paris Cité, CNRS, Laboratoire de Biochimie Théorique, 13 rue Pierre et Marie Curie, 75005, Paris, (France)

Author Contributions

# I. M. A. and W. C. contributed equally.

Notes

The authors declare no competing financial interest.

ACKNOWLEDGEMENTS

This project has received funding from the European Union's Horizon 2020 research and innovation program under the Marie Skłodowska-Curie grant agreement No 860592" and from China Scholarship Council. Computational work was performed using HPC resources from GENCI (grant numbers A0701714 to M.B.) and from LBT- HPC thanks to support from Geoffrey Letessier.

REFERENCES

(1) Nelson, D. L.; Lehninger, A. L.; Cox, M. M. *Lehninger Principles of Biochemistry*; Macmillan, 2008.

(2) Hille, B. *Ionic Channels of Excitable Membranes*, 3rd ed.; Sinauer Sunderland, 2001.

(3) Doyle, D. A.; Cabral, J. M.; Pfuetzner, R. A.; Kuo, A.; Gulbis, J. M.; Cohen, S. L.; Chait, B. T., MacKinnon, R. The Structure of Potassium Channel: Molecular Basis of K^+ Conduction and Selectivity. *Science* **1998**, *280* (5360), 69-77.

(4) Chou, P.-T.; Solntsev, K. M. Photoinduced Proton Transfer in Chemistry and Biology. *J. Phys. Chem. B.* **2015**, *119* (6), 2089-2089.

(5) Springer, A.; Hagen, V.; Cherepanov, D. A.; Antonenko, Y. N.; Pohl, P. Protons Migrate along Interfacial Water without Significant Contributions from Jumps between Ionizable Groups on the Membrane Surface. *Proc. Natl. Acad. Sci.* **2011**, *180* (35), 14461-14466.

(6) Zhang, C.; Knyazev, D. G.; Vereshaga, Y. A.; Ippoliti, E.; Nguyen, T. H.; Carloni, P.; Pohl, P. Water at Hydrophobic Interfaces Delays Proton Surface-to-Bulk Transfer and Provides a Pathway for Lateral Proton Diffusion. *Proc. Natl. Acad. Sci.* **2012**, *109* (25), 9744-9749.

(7) de Groot, B. L.; Grubmuller, H. Water Permeation across Biological Membranes: Mechanism and Dynamics of Aquaporin-1 and GlpF. *Science* **2001**, *294* (5550), 2353-2357.

(8) Agmon, N.; Bakker, H. J., Campen, R. K.; Henchman, R. H.; Pohl, P.; Roke, S.; Thämer, M.; Hassanali, A. Protons and Hydroxide Ions in Aqueous Systems. *Chem. Rev.* **2016**, *116* (13), 7642-7672

(9) Le Duc, Y.; Michau, M.; Gilles, A.; Gence, V.; Legrand, Y.-M.; Van der Lee, A.; Tingry, S.; Barboiu, M. Imidazole-quartet Water and Proton Dipolar Channels. *Angew. Chem.* **2011**, *123* (48), 11568-11574.

(10) Huang, L.-B.; Di Vincenzo, M.; Li, Y.; Barboiu, M. Artificial Water Channels-towards Biomimetic Membranes for Desalination. *Chem. Eur. J.* **2021**, *27*, 2224-2239.

(11) Licsandru, E.; Kocsis, I.; Shen, Y. X.; Murail, S.; Legrand, Y. M.; Van Der Lee, A.; Tsai, D.; Baaden, M.; Kumar, M.; Barboiu, M. Salt-Excluding Artificial Water Channels Exhibiting Enhanced Dipolar Water and Proton Translocation. *J. Am. Chem. Soc.* **2016**, *138*, 5403-5409.

(12) Di Vincenzo, M.; Tiraferri, A.; Musteata, V.-E.; Chisca, S.; Sougrat, R.; Huang, L.-B.; Nunes, S.-P.; Barboiu, M. Biomimetic Artificial Water Channel Membranes for Enhanced Desalination. *Nat. Nanotechnol.* **2021**, *16* (2), 190-196.

(13) Murail, S.; Vasiliu, T.; Neamtu, A.; Barboiu, M.; Sterpone, F.; Baaden, M. Water Permeation across Artificial I-Quartet Membrane Channels: From Structure to Disorder. *Faraday Discuss.* **2018,** *209*, 125-148.

(14) Zhao, H.; Sheng, S.; Hong, Y.; Zeng, H. Proton Gradient-induced Water Transport Mediated by Water Wires Inside Narrow Aquapores of Aquafoldamer Molecules. *J. Am. Chem. Soc.* **2014**, *136*, 14270-14276.

(15) Shen, J.; Fan, J.; Ye, R.; Li, N.; Mu, Y.; Zeng, H. Polypyridine-Based Helical Amide Foldamer Channels: Rapid Transport of Water and Protons with High Ion Rejection. *Angew. Chem. Int. Ed.* **2020**, *59*, 13328-13334.

(16) Shen, J.; Ye, R.; Romanies, A.; Roy, A.; Chen, F.; Ren, C.; Liu, Z.; Zeng, H. Aquafoldamer-Based Aquaporin-like Synthetic Water Channel. *J. Am. Che,. Soc.* **2020**, *142*, 10050-10058.

(17) Roy, A.; Shen, J.; Joshi, H.; Song, W.; Tu, Y.-M.; Chowdhury, R.; Ye, R.; Li, N.; Ren, C.; Kumar, M.; Aksimentiev, A.; Zeng, H. Foldamer-Based Ultrapermeable and Highly Selective Artificial Water Channels that Exclude Protons. *Nat. Nanotechnol.* **2021**, *16* (8), 911-917.

(18) Shen, J.; Roy, A.; Joshi, H.; Samineni, L.; Ye, R.; Tu, Y.-M.; Song, W.; Skiles, M.; Kumar, M.; Aksimentiev, A.; Zeng, H. Fluorofoldamer-Based Salt-and Proton-Rejecting Artificial Water Channels for Ultrafast Water Transport. *Nano Lett.* **2022**, *22* (12), 4831-4838.

(19) Kaucher, M. S.; Peterca, M.; Dulcey, A. E.; Kim, A. J.; Vinogradov, S. A.; Hammer, D. A.; Heiney, P. A.; Percec, V. Selective Transport of Water Mediated by Porous Dendritic Dipeptides. *J. Am. Chem. Soc.* **2007**, *129* (38), 11698-11699.

(20) Percec, V.; Dulcey, A. E.; Balagurusamy, V. S. K.; Miura, Y.; Smirdrkal, J.; Peterca, M.; Nummelin, S.; Edlund, U.; Hudson, S. D.; Heiney, P. A.; Hu, D. A.; Magonov, S. N.; Vinogradov, S. A. Self-Assembly of Amphiphilic Dendritic Dipeptides into

Helical Pores. *Nature*, **2004**, *430*, 764-768.
(21) Feng, W.-X.; Sun, Z.; Zhang, Y.; Legrand, Y.-M.; Petit, E.; Su, C.-Y.; Barboiu, M. Bis-15-Crown-5-Ether-Pillar[5]arene K^+-Responsive Channels. *Org. Lett.* **2017**, *19* (6), 1438-1441.
(22) Strilets, D.; Fa, S.; Hardiagon, A.; Baaden, M.; Ogoshi, T.; Barboiu, M. Biomimetic Approach for Highly Selective Artificial Water Channels Based on Tubular Pillar[5]Arene Dimers. *Angew. Chem. Int. Ed.* **2020**, *59*, 23213-23219.
(23) Barboiu, M. Artificial Water Channels-Incipient Innovative Developments. *Chem. Comm.* **2016**, *52* (33), 5657-5665.
(24) Huang, L. B.; Hardiagon, A.; Kocsis, I.; Jegu, C. A.; Deleanu, M.; Gilles, A.; Van Der Lee, A.; Sterpone, F.; Baaden, M.; Barboiu, M. Hydroxy Channels-Adaptive Pathways for Selective Water Cluster Permeation. *J. Am. Chem. Soc.* **2021**, *143*, 4224-4233.
(25) Mondal, D.; Dandekar, B. R.; Ahmad, M.; Mondal, A.; Mondal, J.; Talukdar, P. Selective and Rapid Water Transportation across a Self-assembled Peptide-Diol Channel via the Formation of a Dual Water Array. *Chem. Sci.* **2022**, *13*, 9614-9623.
(26) Itoh, Y.; Chen, S.; Hirahara, R.; Konda, T.; Aoki, T.; Ueda, T.; Shimada, I.; Cannon, J. J.; Shao, C.; Shiomi, J.; Tabata, K. V.; Noji, H.; Sato, K.; Aida, T. Ultrafast Water Permeation Through Nanochannels with A Densely Flourous Interior Surface. *Science*, **2022**, *376* (6594), 738-743.
(27) Tajkhorshid, E.; Nollert, P.; Jensen, M. Ø.; Miercke, L. J.; O'Connell, J.; Stroud, R. M.; Schulten, K. Control of the Selectivity of the Aquaporin Water Channel Family by Global Orientational Tuning. *Science* **2002**, *296* (5567), 525-530.
(28) Barboiu, M. Artificial Water Channels. *Angew. Chem. Int. Ed.* **2012**, *51* (47), 11674-11676.
(29) Ogoshi, T.; Kanai, S.; Fujinami, S.; Yamagishi, T.; Nakamoto, Y. Para-Bridged Symmetrical Pillar[5] Arenes: Their Lewis Acid Catalysed Synthesis and Host-Guest Property. *J. Am. Chem. Soc.* **2008**, *130* (15), 5022-5023.
(30) Hu, X.-B.; Chen, Z.; Tang, G.; Hou, J.-L.; Li, Z.-T. Single-Molecular Artificial Transmembrane Water Channels. *J. Am. Chem. Soc.* **2012**, *134* (20), 8384-8387.
(31) Si, W.; Xin, P.; Li, Z.-T.; Hou, J.-L. Tubular Unimolecular Transmembrane Channels: Construction Strategy and Transport Activities. *Acc. Chem. Res.* **2015**, *48* (6), 1612-1619.
(32) Si, W.; Chen, L.; Hu, X.; Tang, G.; Chen, Z.; Hou, J.; Li, Z. Selective Artificial Transmembrane Channels for Protons by Formation of Water Wires. *Angew. Chem. Int. Ed.* **2011**, *50* (52), 12564-12568.
(33) Chen, L.; Si, W.; Zhang, L.; Tang, G.; Li, Z.-T.; Hou, J.-L. Chiral Selective Transmembrane Transport of Amino Acids through Artificial Channels. *J. Am. Chem. Soc.* **2013**, *135* (6), 2152-2155.
(34) Si, W.; Li, Z.; Hou, J. Voltage-driven Reversible Insertion into and Leaving from a Lipid Bilayer: Tuning Transmembrane Transport of Artificial Channels. *Angew. Chem. Int. Ed.* **2014**, *53* (18), 4578-4581.
(35) Behera, H.; Yang, L.; Hou, J. Pillar[n] Arenes: Chemistry and their Material Applications. *Chin. J. Chem.* **2020**, *38* (2), 215-217.
(36) Xin, P.; Kong, H.; Sun, Y.; Zhao, L.; Fang, H.; Zhu, H.; Jiang, T.; Guo, J.; Zhang, Q.; Dong, W. Artificial K^+ channels formed by Pillararene-cyclodextrin Hybrid Molecules: Tuning Cation Selectivity and Generating Membrane Potential. *Angew. Chem.* **2019**, *131* (9), 2805-2810.
(37) Fa, S.; Sakata, Y.; Akine, S.; Ogoshi, T. Non-Covalent Interactions Enable the Length-Controlled Generation of Discrete Tubes Capable of Guest Exchange. *Angew. Chem.* **2020**, *132* (24), 9395-9399.
(38) Buffet, K.; Nierengarten, I.; Galanos, N.; Gillon, E.; Holler, M.; Imberty, A.; Matthews, S. E.; Vidal, S.; Vincent, S. P.; Nierengarten, J. Pillar [5] Arene-based Glycoclusters: Synthesis and Multivalent Binding to Pathogenic Bacterial Lectins. *Chem. Eur. J.* **2016**, *22* (9), 2955-2963.
(39) Vincent, S. P.; Buffet, K.; Nierengarten, I.; Imberty, A.; Nierengarten, J. -F.. Biologically Active Heteroglycoclusters Constructed on a Pillar [5] Arene-containing [2] Rotaxane Scaffold. *Chem. Eur. J.* **2016**, *22* (1), 88-92.
(40) Mohy El Dine, T.; Jimmidi, R.; Diaconu, A.; Fransolet, M.; Michiels, C.; De Winter, J.; Gillon, E.; Imberty, A.; Coenye, T.; Vincent, S. P. Pillar [5] Arene-Based Polycationic Glyco [2] Rotaxanes Designed as Pseudomonas Aeruginosa Antibiofilm Agents. *J. Med. Chem.* **2021**, *64* (19), 14728-14744.
(41) Nierengarten, I.; Buffet, K.; Holler, M.; Vincent, S. P.; Nierengarten, J.-F. A Mannosylated Pillar [5] Arene Derivative: Chiral Information Transfer and Antiadhesive Properties against Uropathogenic Bacteria. *Tetrahedron Lett.* **2013**, *54* (19), 2398-2402.
(42) Tikad, A.; Fu, H.; Sevrain, C. M.; Laurent, S.; Nierengarten, J. -F; Vincent, S. P. Mechanistic insight into Heptosyltransferase Inhibition by Using Kdo Multivalent Glycoclusters. *Chem. Eur. J.* **2016**, *22* (37), 13147-13155.
(43) Ogoshi, T.; Kakuta, T.; Yamagishi, T. Applications of Pillar [n] Arene-based Supramolecular Assemblies. *Angew. Chem. Int. Ed.* **2019**, *58* (8), 2197-2206.
(44) Chen, W.; Vincent, S.P. Coppilar [5] Arene Chemistry: Synthesis and Applications. *Synthesis* **2023**, *55*, 246-262.
(45) Shen, Y. X.; Si, W.; Erbakan, M.; Decker, K.; De Zorzi, R.; Saboe, P. O.; Kang, Y. J.; Majd, S.; Butler, P. J.; Walz, T.; Aksimentiev, A.; Hou, J. L.; Kumar, M. Highly Permeable Artificial Water Channels than can Self-assemble into Two-Dimensional Arrays. *Proc. Natl. Acad. Sci. U.S.A.* **2015**, *112*, 9810-9815.
(46) Nierengarten, I.; Guerra,S.; Holler, M.; Nierengarten, J. F.; Deschenaux, R. Building Liquid Crystals from the 5-Fold Symmetrical Pillar [5] Arene core. *Chem Commun.* **2012**, *48* (65), 8072-8074.
(47) Chen, W.; Mohy El Dine, T.; Vincent, S.P. Synthesis of Functionalized Copillar [4+1] Arenes as Rotaxane as Heteromultivalent Scaffolds. *Chem. Commun.* **2021**, *54*, 492-495.
(48) Petitjean, S. J. L.; Chen, W.; Koehler, M.; Jimmidi, R.; Yang, J.; Mohammed, D.; Juniku, B.; Stanifer, M. L.; Boulant, S.; Vincent, S. P.; Alsteens, D. Multivalent 9-O-Acetylated-Sialic Acid Glycoclusters as Potent Inhibitors for SARS-CoV-2 Infection. *Nat. Comm.* **2022**, *13*, 2564.
(49) Guérin, C.; Jean-Gérard, L.; Octobre, G.; Pascal, S.; Maury, O.; Pilet, G.; Ledoux, A.; Andrioletti, B. Bis-Triazolyl BODIPYs: A Simpli Dye with Strong Red-Light Emission. *RSC Avd.* **2015**, *5* (93), 76342-76345.
(50) Yang, C.; Flynn, J. P.; Niu, J. Facile Synthesis of Sequence-Regulated Synthetic Polymers Using Orthogonal SuFEx and CuAAC Click Reactions. *Angew. Chem. Int. Ed.* **2018**, *57* (49), 16194-16199.
(51) Wasser, J.; Gaspar, B.; Nambu, H.; Carreira, E. M. Hydrazines and Azides via the Metal-Catalyzed Hydrohydrazination and Hydroazidation of Olefins. *J. Am. Chem. Soc.* **2006**, *128* (35), 11693-11712.
(52) Willoughby, D.; Thomas, R. C.; Schwiening, C. J. Comparison of Simultaneous pH Measurements Made with 8-Hydroxypyrene-1,3,6-Trisulphonic Acid (HPTS) and pH-Sensitive Microelectrodes in Snail Neurons. *Pflüg. Arch.* **1998**, *436*, 615-622.
(53) Spry, D.; Goun, A.; Fayer, M. D. Deprotonation Dynamics and Stokes Shift of Pyranine (HPTS). *J. Phys. Chem. A.* **2007**, *111* (2), 230-237.
(54) Matile, S.; Sakai, N.; Hennig, A. Transport Experiments in Membranes. *Supramol. Chem. Mol. Nanomater.* **2012**, 473-500.
(55) Nandi, R.; Amdursky, N. The Dual Use of the Pyranine (HPTS) Fluorescent Probe: A Ground-State pH Indicator and an Excited-State Proton Transfer Probe. *Acc. Chem. Res.* **2022**, *55* (18), 2728-2739.
(56) Yan, Z.-J.; Wang, D.; Ye, Z.; Fan, T.; Wu, G.; Deng, L.; Yang, L.; Li, B.; Liu, J.; Ma, T.; Dong, C.; Li, Z.-T.; Xiao, L.; Wang, Y.; Wang, W.; Hou, J.-L. Artificial Aquaporin that Restores Wound Healing of Impaired Cells. *J. Am. Chem. Soc.* **2020**, *142* (37), 15638-15643.
(57) Xiao, Q.; Fan, T.; Wang, Y.; Li, Z.-T.; Hou, J. L.; Wang, Y. Artificial Water Channel that Couples with Cell Protrusion Formation. *CCS Chem.* **2023**, 1-8.
(58) Hu, F.; Luo, W.; Hong, M. Mechanisms of proton conduction and gating in influenza M2 proton channels from solid-state NMR. *Science* **2010**, *330*, 505-508.

(59) Brown, L.S.Light-driven proton transfers and proton transport by microbial rhodopsins - A biophysical perspective, *BBA - Biomembranes*, **2022**, *1864*, 183867.
(60) Yan, T.; Liu, S.; Xu, J.; Sun, H.; Yu, S.; Liu, J. Unimolecular Helix-Based Transmembrane Nanochannel with a Smallest Luminal Cavity of 1 Å Expressing High Proton Selectivity and Transport Activity. *Nano Lett.* **2021**, *21*, 10462- 10468.
(61) J. Shen, R. Ye, Z. Liu, H. Zeng, Hybrid Pyridine–Pyridone Foldamer Channels as M2-Like Artificial Proton Channels. *Angew. Chem. Int. Ed.* **2022**, *61*, e202200259.

TOC GRAPHIC